Ultraviolet-laser atom-probe tomographic three-dimensional atom-by-atom mapping of isotopically modulated Si nanoscopic layers

Oussama Moutanabbir,[1,a)] Dieter Isheim,[2,b)] David N. Seidman,[2,c)] Yoko Kawamura,[3] and Kohei M. Itoh[3]

[1]*Max Planck Institute of Microstructure Physics, Weinberg 2, 06120 Halle (Saale), Germany*
[2]*Department of Materials Science and Engineering, Northwestern University, Evanston, IL 60208-3108, USA*
[3]*School of Fundamental Science and Technology, Keio University, 3-14-1 Hiyoshi, Kohoku-ku, Yokohama 223-8522, Japan*

(Received 2 September 2010; accepted 6 December 2010; published online 7 January 2011)

Using ultraviolet-laser assisted local-electrode atom-probe (UV-LEAP) tomography, we obtain three-dimensional (3D) atom-by-atom images of isotopically modulated ^{28}Si and ^{30}Si ultrathin layers having thicknesses in the range of 5–30 nm. The 3D images display interfaces between the different monoisotopic layers with an interfacial width of ~1.7 nm, thus demonstrating a significant improvement over isotope mapping achievable using secondary-ion mass-spectrometry or even visible laser-assisted atom-probe tomography. This sharpness is attributed to reduced thermal effects resulting from using a highly focused UV laser beam. Our findings demonstrate that UV-LEAP tomography provides the high accuracy needed to characterize, at the subnanometer scale, the emerging isotopically programmed nanomaterials. *© 2011 American Institute of Physics*. [doi:10.1063/1.3531816]

The introduction of stable semiconductor isotopes as an additional degree of complexity in nanofabrication processes creates a wealth of opportunities for the manipulation of the properties of emerging nanomaterials.[1–3] Moreover, the absence of any significant chemical, electrical, structural, or mechanical driving forces among the isotopes makes possible the study of atomic transport phenomena on the nanoscale.[4] Extensive investigations over the past two decades have demonstrated that the physical properties of bulk semiconductors are drastically changed by manipulating the relative proportions of their stable isotopes.[1,5,6] In general, isotope-related effects are caused either by the influence of the atomic mass on the lattice dynamics or by differences in nuclear properties among isotopes. For example, large isotopic effects are observed near the thermal conductivity maximum due to the impact of mass disorder on phonon scattering.[1,6,7] Additionally, the atomic mass also influences the band gap energy.[1,5,6] This phenomenon was recently utilized to engineer diamond isotopic homojunctions enabling charge-carrier confinement in a chemically homogeneous material.[3]

In spite of the crucial information they could provide, there are only a few predominantly theoretical studies on the influence of isotopic content on the physical properties of isotopically engineered nanostructures. For instance, recent simulations demonstrate that the thermal conductivity of Si nanowires is reduced exponentially by isotopic impurities at room temperature,[7] and the figure of merit of a $^{28}Si_{0.5}{}^{29}Si_{0.5}$ nanowire is ~31% greater than that of an isotopically pure nanowire.[7] No experimental investigation has, however, been performed to test these calculations. Recently, the influence of isotope impurities on heat and electronic transports was investigated in carbon and BN nanotubes.[8–10]

From both fundamental and technological standpoints, it is of compelling importance to explore experimentally isotope-related effects in semiconductor-based nanomaterials. Besides the meticulous control over nanofabrication processes, tackling this area of research also requires characterization techniques that are sensitive to one of the isotopic properties, atomic mass, or nuclear properties, or to phonon-related phenomena. These techniques should also offer the spatial resolution needed to probe nanoscale structures. In this letter, we demonstrate that ultraviolet (UV) laser-assisted local-electrode atom-probe (UV-LEAP) tomography provides the spatial resolution, mass resolving power ($m/\Delta m$), and signal-to-noise (S/N) ratio needed to characterize accurately isotopically engineered semiconductor nanomaterials. The use of LEAP tomography to characterize the distribution of Si isotopes was first reported by Shimizu *et al.*[11] In that research, however, the use of a visible laser to assist the evaporation led to limited analytical and spatial resolution.

An atom-probe tomograph consists of a field-ion microscope coupled directly to a special time-of-flight mass spectrometer, which permits the identification of the mass-to-charge-state ratios of individual evaporated ions in addition to their (x,y,z) coordinates in a specimen in real space, with subnanometer resolution.[12–14] We utilize an UV laser-assisted LEAP (LEAP 4000XSi (Cameca, Madison, WI). Pulsed-evaporation of individual atoms is achieved employing focused picosecond UV (wavelength $\lambda = 355$ nm) laser pulses with a laser beam waist of <5 μm at the e^{-2} diameter. The evaporation rate (ion pulse^{-1}), the laser pulse repetition-rate, and energy pulse^{-1} were 0.01, 500 kHz, and 40 pJ, respectively. This UV laser pulse-energy was utilized to minimize local heating of specimens. The 3D reconstructions were performed using Cameca's IVAS program.

The investigated samples consist of isotopically modulated Si multilayers grown by solid-source molecular beam epitaxy using ^{28}Si and ^{30}Si enriched isotopes.[15] 2 in. diam-

a)Electronic mail: moutanab@mpi-halle.mpg.de.
b)Electronic mail: sheim@northwestern.edu.
c)Electronic mail: d-seidman@northwestern.edu.

 © 2011 American Institute of Physics

Downloaded 07 Jan 2011 to 131.113.64.180. Redistribution subject to AIP license or copyright; see http://apl.aip.org/about/rights_and_permissions

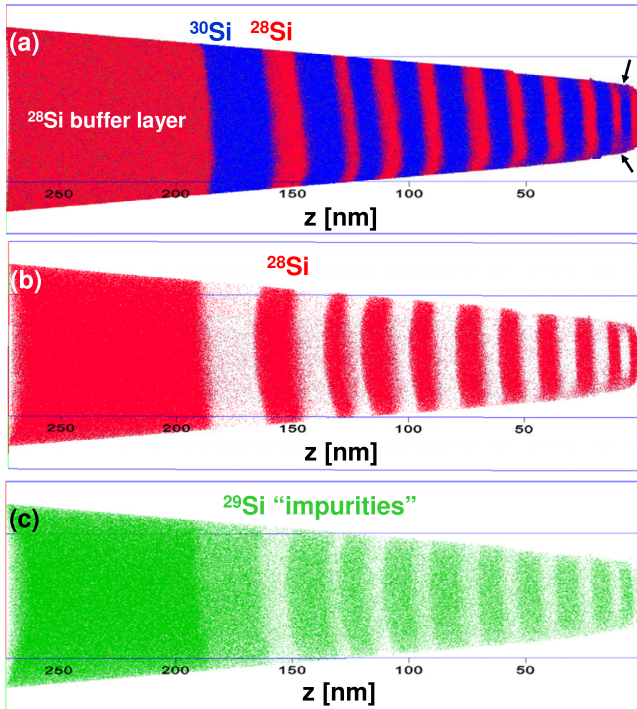

FIG. 1. (Color online) Typical UV-LEAP tomographic 3D images of: (a) isotopically modulated ^{28}Si/^{30}Si layers, (b) ^{28}Si isotope-only 20% of the ^{28}Si atoms are displayed for clarity, and (c) ^{29}Si isotope. The arrows in (a) indicate isotopically mixed regions due to the exposure to Ga ions during FIB specimen preparation.

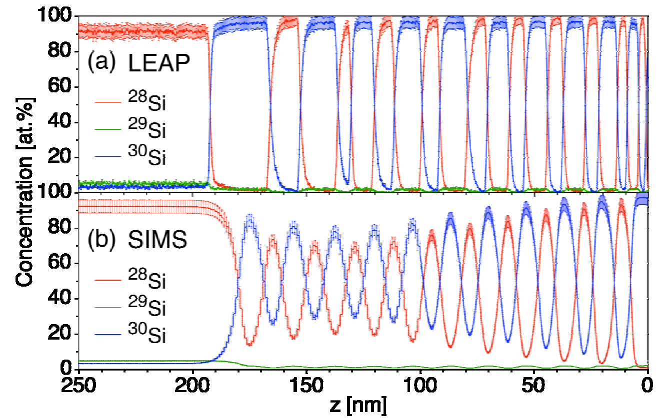

FIG. 2. (Color online) (a) Concentration depth profiles of the three Si isotopes, ^{28}Si, ^{29}Si, and ^{30}Si, calculated from the UV-LEAP tomographic map in Fig. 1(a). (b) SIMS concentration profiles of ^{28}Si, ^{29}Si, and ^{30}Si isotopes measured for the identical sample. (c) Comparison of ^{28}Si concentration profiles measured using UV-LEAP tomography and SIMS. The sample used in SIMS analysis was capped with a ^{30}Si layer.

eter *n*-type wafers, high-resistivity float-zone Si(001), were employed as substrates. After wet chemical cleaning in H_2SO_4 and H_2O_2 solutions and a dip in an HF dilute solution, the wafers were preannealed at 850 °C, and then followed by growth of an ~100 nm-thick ^{28}Si buffer layer at 650 °C. Isotopically modulated ^{28}Si and ^{30}Si ultrathin layers having thicknesses in the range of 5–30 nm were grown at the latter temperature. The total thickness of the ^{28}Si/^{30}Si alternating layers is ~200 nm. These layers are defect-free as confirmed by cross-sectional transmission electron microscopy. LEAP tomographic specimens were prepared using a Helios dual-beam focused-ion beam (FIB) microscope (FEI Co., Hillsboro, Oregon) in conjunction with a micromanipulator. To prevent radiation damage produced by Ga ions during FIB nanomachining, a ~40 nm-thick Ni protective cap layer was deposited on ^{28}Si/^{30}Si samples. Needlelike specimens with a tip radius of ~20 nm were fabricated using the FIB-based lift-out method and attached to Si microposts on coupons. The microtips were subsequently inserted into the LEAP tomograph's ultrahigh-vacuum chamber and cooled to 60 K prior to pulsed laser-assisted evaporation analyses. The microtips were maintained at a positive potential, while the evaporation of atoms was triggered by UV laser pulses.

Figure 1(a) displays a typical 3D LEAP tomographic atom-by-atom reconstructed image of isotopically modulated ^{28}Si and ^{30}Si layers. The formation of Si–H complexes is negligible in our measurement. Detailed analysis of the recorded mass spectra resulted in an upper limit of 0.01 at. % for a potential contribution of Si–H ions to Si isotopes peaks. The ^{28}Si buffer layer is also displayed in the image as well as the distribution of ^{29}Si "impurities" observed in both ^{28}Si and ^{30}Si layers. A small concentration of ^{28}Si is also observed in the ^{30}Si layers and vice versa; Fig. 1(b) depicting the 3D map of ^{28}Si. The presence of the isotopic "impurities" in essentially monoisotopic layers is related to the enrichment level of the different sources used for growing the multilayers. From Fig. 1(a), we estimate the isotopic concentration of the ^{28}Si-enriched source to be (98.63 ± 0.48)at. % ^{28}Si, (0.44 ± 0.14)at. % ^{29}Si, and (0.93 ± 0.38)at. % ^{30}Si; whereas the isotopic composition of the ^{30}Si-enriched source is (1.02 ± 0.20)at. % ^{28}Si, (2.01 ± 0.27)at. % ^{29}Si, and (96.97 ± 0.40)at. % ^{30}Si.

The concentration depth profiles calculated from the 3D image in Fig. 1(a) are exhibited in Fig. 2(a). It is noteworthy that the profiles clearly resolve the monoisotopic layers. Independent of the thickness, the profiles display plateau regions for each individual isotopic layer, demonstrating that the full concentration amplitude between the layers has been resolved. The interfacial regions between the layers are also resolved with a very sharp transition. To appreciate this interfacial abruptness, an identical sample was analyzed using secondary-ion mass-spectrometry (SIMS) (PHI Adept 1010). A SIMS analysis was performed using 750 eV Cs^+ primary ions at an incidence angle of 60° with respect to the normal to the surface at a current of 50 nA, Fig. 2(b). The striking observation is that the SIMS data exhibit broader profiles with more diffuse interfaces than the atom probe tomography (APT) profiles. Also, the SIMS data do not exhibit plateau regions, that is, the concentration amplitude between the isotopic layers is not fully resolved. Additionally, the interfacial width of the probed layers is also less resolved by SIMS due to its limited depth resolution. A similar conclusion is drawn from a comparative analysis of Si/SiGe multilayers.[16] These observations demonstrate that UV-LEAP tomography has significantly better spatial and analytical resolutions compared to SIMS. This improved 3D isotopic imaging is clearly seen in Fig. 3(a), displaying the 3D isotopic map in a $30\times30\times30$ nm^3 volume extending from 35 to 65 nm depth of all isotopes including the 50 at. % ^{28}Si isoconcentration surfaces. The interfacial width is estimated by calculating the separation between 10% and 90% concentration points at the ^{28}Si/^{30}Si interface, using a cubic spline fit to the profile. Figure 3(b) shows the result of the fit at $z=\sim37$ nm indicating an interfacial width of 1.50 ± 0.01 nm. The mean in-

Downloaded 07 Jan 2011 to 131.113.64.180. Redistribution subject to AIP license or copyright; see http://apl.aip.org/about/rights_and_permissions

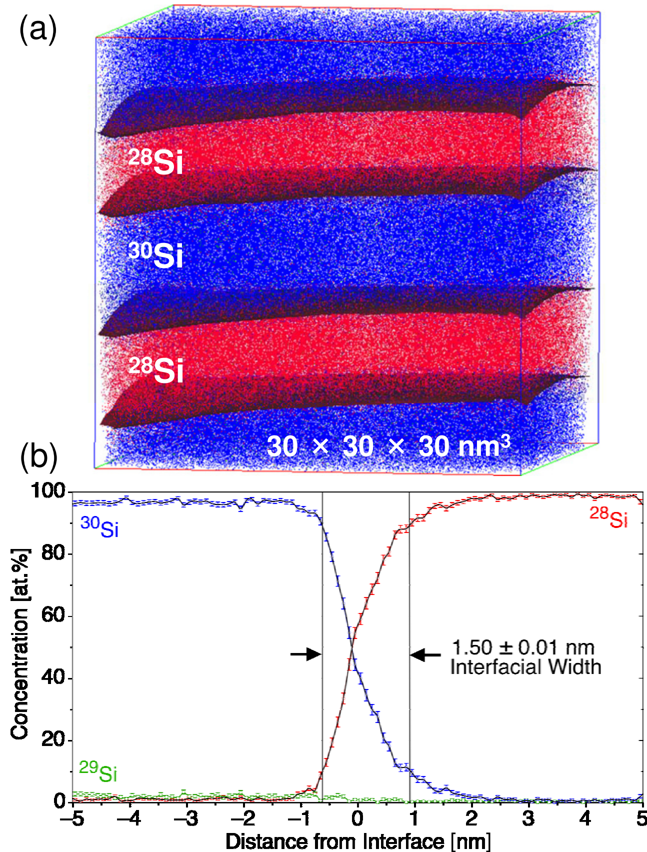

FIG. 3. (Color online) (a) 3D UV-LEAP tomographic isotopic map of a $30\times30\times30$ nm^3 volume from 35 to 65 nm depth of all isotopes. 50 at. % ^{28}Si isoconcentration surfaces are superposed to delineate the interfaces. (b) The estimated interfacial width. The solid-black lines are the best fit of experimental data employing a cubic spline-function.

terfacial width averaged over several interfaces is 1.70 ± 0.19 nm.

It is noteworthy that the use of highly focused UV lasers is uncommon and the vast majority of the currently available laser-assisted APT systems utilize lasers in the visible spectrum (green or blue). It was demonstrated that green laser-assisted APT yields isotopic concentration profiles with a decay length of 2.1 nm/decade.[11] In our analyses, employing UV-assisted LEAP [Fig. 2(a)], the average decay length is 0.6 nm/decade. The fact that the highly focused UV laser-assisted ATP outperforms visible laser-assisted APT implies that the laser wavelength and focus diameter play a critical role in the spatial and analytical resolutions, and $m/\Delta m$ of UV laser-assisted LEAP tomography. Although the exact mechanism by which laser-induced evaporation of atoms occurs is debatable,[17,18] the physical mechanisms that are generally accepted are related to local heating of the specimen by the laser beam with an energy per pulse that is typically less than 5 nJ.[12] This local heating process implies that an atom is thermally excited over the Schottky hump produced by the positive electric potential applied to a microtip. Bunton *et al.*[19] demonstrate that a smaller laser spot combined with good thermal conductivity of a sample results in efficient cooling. The use of the UV laser with a highly focused beam, instead of a visible laser, leads to a more localized heating of the microtip due to its smaller laser beam diameter. A critical difference in the present case also comes from the reduced penetration depth of the UV laser in Si. The penetration depth is only ~10 nm at $\lambda=355$ nm, compared to ~980 nm at $\lambda=532$ nm. This radical difference in the adsorption of the laser energy may also contribute to the more confined heating with the UV laser beam. The local energy-density is increased, and therefore the thermal gradient, which results in a larger flux of heat away from a microtip's apex. This translates to less extensive thermal tails, higher S/N ratios, and better $m/\Delta m$ values, thereby improving concomitantly spatial resolution and minimum concentration detectability.

In conclusion, we have demonstrated 3D atom-by-atom imaging of isotopically modulated ^{28}Si and ^{30}Si ultrathin layers using UV laser-assisted LEAP tomography. The obtained highly resolved nanomaps with an interfacial width of 1.70 ± 0.19 nm between different monoisotopic layers demonstrate a significant improvement over isotopic mapping achievable using SIMS or visible laser-assisted APT. The reduced thermal effects are suggested to play a key role in the improved spatial resolution observed using UV-LEAP tomography. Our results demonstrate that UV-LEAP tomography is a powerful and accurate instrument in the emerging field of isotopically engineered semiconductor nanomaterials.

O.M. acknowledges funding from the German Ministry of Education and Research (BMBF) under Contract Nos. 01BU0624 (CRYSGAN) and 13 N 9881 (DECISIF). This research was partially supported by the U.S.-Israel Binational Science Foundation (D.I. and D.N.S.). The LEAP tomograph was purchased with funding from the NSF-MRI and ONR-DURIP programs. The work at Keio has been supported in part by Special Coordination Funds for Promoting Science and Technology, in part by Grant-in-Aid for Scientific Research by MEXT, and a Grant-in-Aid for the Keio Global Center of Excellence for High-Level Global Cooperation.

[1] J. W. Ager III and E. E. Haller, Phys. Status Solidi A **203**, 3550 (2006).
[2] O. Moutanabbir, S. Senz, Z. Zhang, and U. Gösele, Nano Today **4**, 393 (2009).
[3] H. Watanabe, C. E. Nebel, and S. Shikata, Science **324**, 1425 (2009).
[4] O. Moutanabbir, S. Miyamoto, E. E. Haller, and K. M. Itoh, Phys. Rev. Lett. **105**, 026101 (2010).
[5] M. Cardona and M. L. W. Thewalt, Rev. Mod. Phys. **77**, 1173 (2005).
[6] V. G. Plekhanov, Prog. Mater. Sci. **51**, 287 (2006).
[7] G. Zhang and B. Li, Nanoscale **2**, 1058 (2010).
[8] C. W. Chang, A. M. Fennimore, A. Afanasiev, D. Okawa, T. Ikuno, H. Garcia, D. Li, A. Majumdar, and A. Zettl, Phys. Rev. Lett. **97**, 085901 (2006).
[9] I. Savić, N. Mingo, and D. A. Stewart, Phys. Rev. Lett. **101**, 165502 (2008).
[10] N. Vandecasteele, M. Lazzeri, and F. Mauri, Phys. Rev. Lett. **102**, 196801 (2009).
[11] Y. Shimizu, Y. Kawamura, M. Uematsu, K. M. Itoh, M. Tomita, M. Sasaki, H. Uchida, and M. Takahashi, J. Appl. Phys. **106**, 076102 (2009).
[12] D. N. Seidman, Annu. Rev. Mater. Res. **37**, 127 (2007).
[13] D. N. Seidman and K. Stiller, MRS Bull. **34**, 717 (2009).
[14] M. K. Miller, *Atom-Probe Tomography: Analysis at the Atomic Level* (Plenum, New York, 2000).
[15] T. Kojima, R. Nebashi, K. M. Itoh, and Y. Shiraki, Appl. Phys. Lett. **83**, 2318 (2003).
[16] S. Koelling, M. Gilbert, J. Goossens, A. Hikavyy, O. Richard, and W. Vandervorst, Appl. Phys. Lett. **95**, 144106 (2009).
[17] B. Gault, F. Vurpillot, A. Bostel, A. Menand, and B. Deconihut, Appl. Phys. Lett. **86**, 094101 (2005).
[18] A. Cerezo, G. D. W. Smith, and P. H. Clifton, Appl. Phys. Lett. **88**, 154103 (2006).
[19] J. H. Bunton, J. D. Olson, D. R. Lenz, and T. F. Kelly, Microsc. Microanal. **13**, 418 (2007).

Downloaded 07 Jan 2011 to 131.113.64.180. Redistribution subject to AIP license or copyright; see http://apl.aip.org/about/rights_and_permissions